# CHAPTER 5

# PHYSICAL AND ELECTRICAL PROPERTIES OF MODIFIED PZN-PZT COMPOSITIONS

This chapter describes the investigation of physical and electrical properties of modified PZN-PZT compositions. There are three part, (1) the effect of $MnO_2$ addition on properties of PZN-PZT ceramics, (2) the effect of $Fe_2O_3$ addition on properties of PZN-PZT ceramics, and (3) Comparison between $Fe_2O_3$ and $MnO_2$ addition on properties of PZN-PZT-based ceramics. The scope of measurement is defined and the results of dielectric, piezoelectric and ferroelectric properties are shown.

## 5.1. Effect of $MnO_2$ addition on properties of PZN-PZT ceramics

Fan and Kim [97] investigated $Pb(Zn_{1/3}Nb_{2/3})_{0.5}(Zr_{0.47}Ti_{0.53})_{0.5}O_3$ ceramics with composition close to the morphotropic phase boundary (MPB) and clarified that the ceramics have large electromechanical coupling factor $k_p$. However, the mechanical quality factor $Q_m$ is too low to permit their use as high power piezoelectric devices. It is necessary to improve $Q_m$ as much as possible for suppressing the generation of heat during operation. To develop materials suitable for multilayer piezoelectric transformers and actuators with high $d_{33}$, high $k_p$ and $Q_m$, it is necessary to add some dopants on PZN–PZT based ceramics to optimize the piezoelectric properties for device applications[9, 45, 74, 85]. The influence of

various substitutions on the B-site of $Pb(Zr,Ti)O_3$ perovskite has been widely investigated to optimize the piezoelectric properties [37, 93, 98-101].

Previously, all commercial piezoelectric devices employ $Pb(Zr,Ti)O_3$ (PZT)-based formulations, close to the morphotropic phase boundary (MPB). The MPB composition is modified by the acceptor and donor ions to yield high piezoelectric properties with low losses. Regarding the Mn doping effect since Mn ions can have various valencies from $Mn^{4+}$ to $Mn^{2+}$, Mn-ions are well known to be effective in very small amounts for improving the reliability of ceramic capacitors. The enhanced properties are expected to be due to the distribution of $Mn^{2+}$, $Mn^{3+}$, and $Mn^{4+}$ on B-sites[102-104, 108]. Mn incorporated on the B sites would act as a lower valent species on a higher valent site. Accordingly, oxygen vacancies would be created for charge compensation, imparting polarization pinning and ‘‘hard’’ characteristics, i.e., an increase in $Q_m$ value [101-104].

In this section, in order to develop PZN-PZT based ceramics for a piezoelectric transformer application, we investigate the effect of $MnO_2$ addition on structure, and electrical properties of $0.2Pb(Zn_{1/3}Nb_{2/3})O_3$-$0.8Pb(Zr_{1/2}Ti_{1/2})O_3$ ceramics. The purpose of this study is to obtain ceramics with higher $d_{33}$, $k_p$ and $Q_m$, which are especially important from the viewpoint of the development of practical piezoelectric materials.



### 5.1.1. Experimental procedure

The specimens studied were fabricated according to the formula: $0.2Pb(Zn_{1/3}Nb_{2/3})O_3$-$0.8Pb(Zr_{1/2}Ti_{1/2})O_3$ + $x$ wt% $MnO_2$, where x= 0.1, 0.3, 0.5, 0.7

and 0.9. Raw materials of PbO, $ZrO_2$, $TiO_2$, ZnO, $Nb_2O_5$ and $MnO_2$ with >99% purity were used to prepare samples by a conventional mixed oxide process. The starting powders were mixied by zirconia ball media with isopropanal as a medium in a polyethylene jar for 30 min via vibro-milling technique. The mixed slurry was dried and calcined at 900$^{o}$C for 2h. The calcined powders were ball-milled again with additives and consolidated into disks of 12.5 mm diameter using isostatic pressing about 150 MPa. PbO-rich atmosphere sintering of the ceramics was performed in a high-purity alumina crucible at 1200 °C for 2h. Physical and electrical characteristics of the prepared ceramics were investigated with similar procedures described earlier in Chapters 3 and 4.

## 5.1.2. Results and discussion

### 5.1.2.1. Crystal structure, phase formations and microstructure

Perovskite phase formation, crystal structure and lattice parameter were determined by XRD at room temperature. The XRD patterns of $0.2Pb(Zn_{1/3}Nb_{2/3})O_3$-$0.8Pb(Zr_{1/2}Ti_{1/2})O_3$, with the addition of 0–0.9 wt% $MnO_2$ are shown in Fig.5.1, showing perovskite structure for all compositions. The pyrochlore phase is not observed in this system. In the XRD patterns, the crystal structure of the specimens appears clearly to change to rhombohedral side across MPB with increasing amount of $MnO_2$ around 0.5 wt%. It has been reported [98, 101] that manganese coexists mainly in the $Mn^{2+}$ and $Mn^{3+}$states, which then enter into the perovskite structure of $BO_6$ octahedron to substitute for the B-site ion (e.g., $Ti^{4+}$and $Zr^{4+}$).

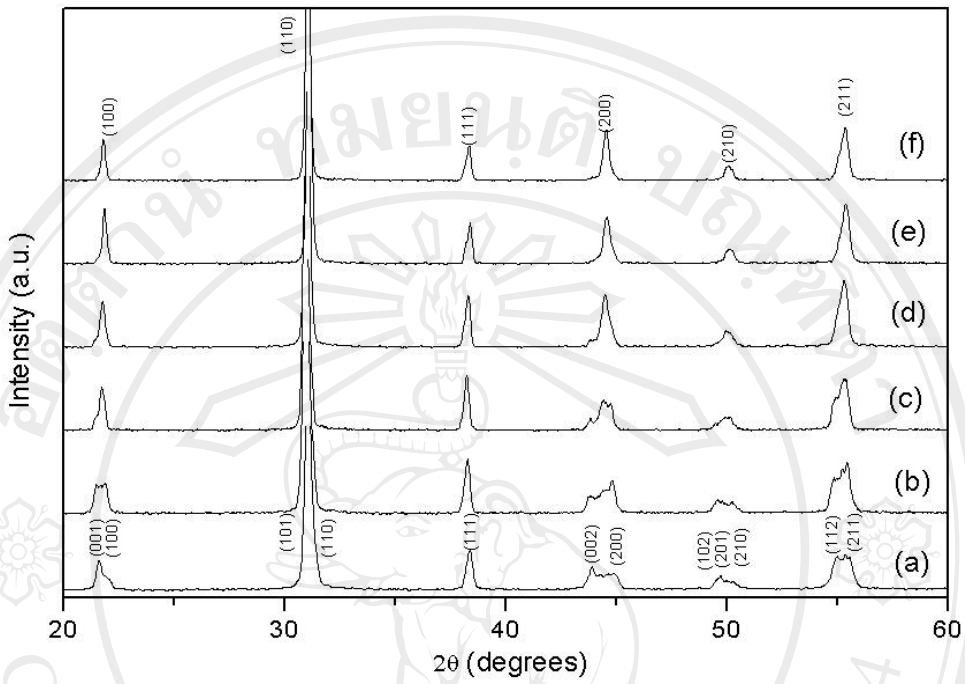


**Figure 5.1** XRD patterns of the samples sintered at 1200°C for 2h in of 0.2PZN–0.8PZT + *x* wt% $MnO_2$ ceramics: (a) *x* =0, (b) *x* =0.1, (c) *x* =0.3, (d) *x* =0.5, (e) *x* =0.7 and (f) *x* =0.9.

Figure 5.2 shows SEM photographs of the surfaces of $0.2Pb(Zn_{1/3}Nb_{2/3})O_3$-$0.8Pb(Zr_{1/2}Ti_{1/2})O_3$ ceramics doped with 0–0.9 wt% $MnO_2$. As shown in Figs. 5.2 (a-b), the grain sizes of ceramics are increased with an increasing amount of $MnO_2$ addition. Similar observations have been reported [107]. Further increasing in $MnO_2$ content gives rise to an in homogeneous grain size. However, the SEM micrograph in Fig.5.2(c-f) show that a higher porosity level is observed when the amount of $MnO_2$ is increased [105]. The above results are obviously consistent with the change in the bulk density with $MnO_2$ content for Mn-doped $0.2Pb(Zn_{1/3}Nb_{2/3})O_3$-$0.8Pb(Zr_{1/2}Ti_{1/2})O_3$ ceramics. It can clearly be seen from Fig. 5.2 that the ceramics

have high densities in the $MnO_2$ addition range of 0–0.5 wt%. It is believed that manganese ions are mainly incorporated into the lattice, but if the addition is above 0.5 wt%, manganese ions will accumulate at the grain boundaries [104]. These inferences are obviously consistent with the changes mentioned above in the microstructures. The micrographs also show that the grain size of the ceramics varies considerably, as listed in Table 5.1.

**Table 5.1** Physical Properties of 0.2PZN–0.8PZT + *x* wt% $MnO_2$ ceramics

| *x* | Density (g/cm$^3$) | Grain size range(μm) | Average grain size (μm) |
|---|---|---|---|
| 0 | 7.826 | 0.5 - 2.0 | 1.726 |
| 0.1 | 7.849 | 1.5 – 6.0 | 4.131 |
| 0.3 | 7.897 | 1.0 – 3.0 | 2.991 |
| 0.5 | 8.028 | 0.5 – 2.0 | 2.116 |
| 0.7 | 7.718 | - | - |
| 0.9 | 7.653 | - | - |

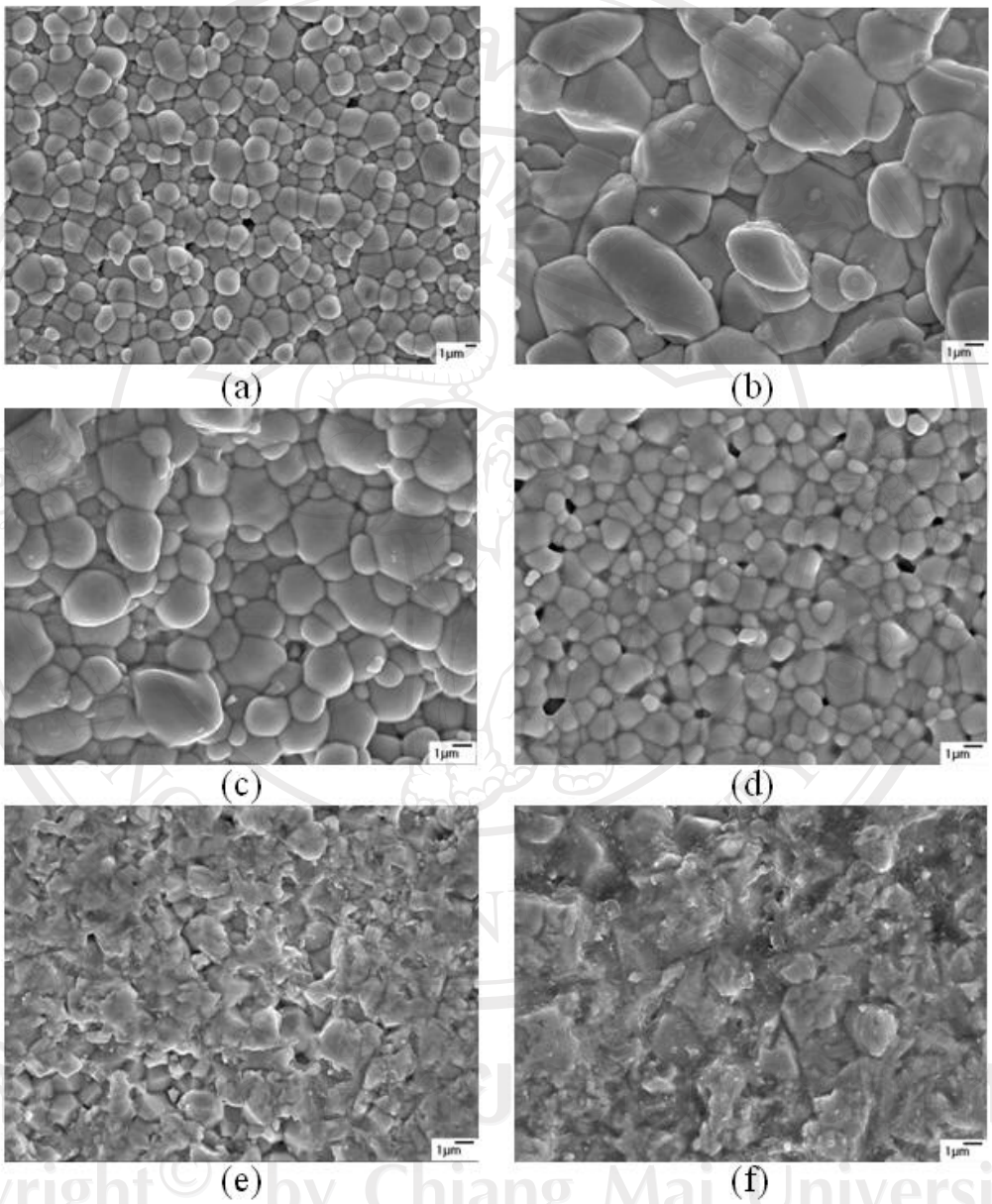


**Figure 5.2** SEM images of the specimens sintered surface of 0.2PZN–0.8PZT + *x* wt% $MnO_2$ ceramics at 1200°C for 2h;(a) *x* =0, (b) *x* =0.1, (c) *x* =0.3, (d) *x* =0.5, (e) *x* =0.7 and (f) *x* =0.9.

#### 5.1.2.2. Dielectric properties

The temperature and frequency dependence of the dielectric constant ($\varepsilon_r$) and dielectric loss tangent (tan $\delta$) for 0.2PZN–0.8PZT + *x* wt% $MnO_2$, *x* = 0, 0.1, 0.3, 0.5, 0.7 and 0.9 are shown in Fig. 5.3. The maximum dielectric constant at 1 kHz ($\varepsilon_m$ @ 1 kHz) is listed in Table 5.2. Dielectric behaviors show strong increase in frequency-dependence of dielectric constant and dielectric loss which increased amount of $MnO_2$. This may be caused from oxygen vacancies and conducting regions near grain boundaries when increasing $MnO_2$ [108]. The variation of the Curie temperature ($T_c$) as a function of composition *x* is shown in Fig 5.4. The Curie temperature of 0.2PZN–0.8PZT + *x* wt% $MnO_2$ system can be varied over a wide range from 310 to 340°C by controlling the addition of $MnO_2$ content in the system.

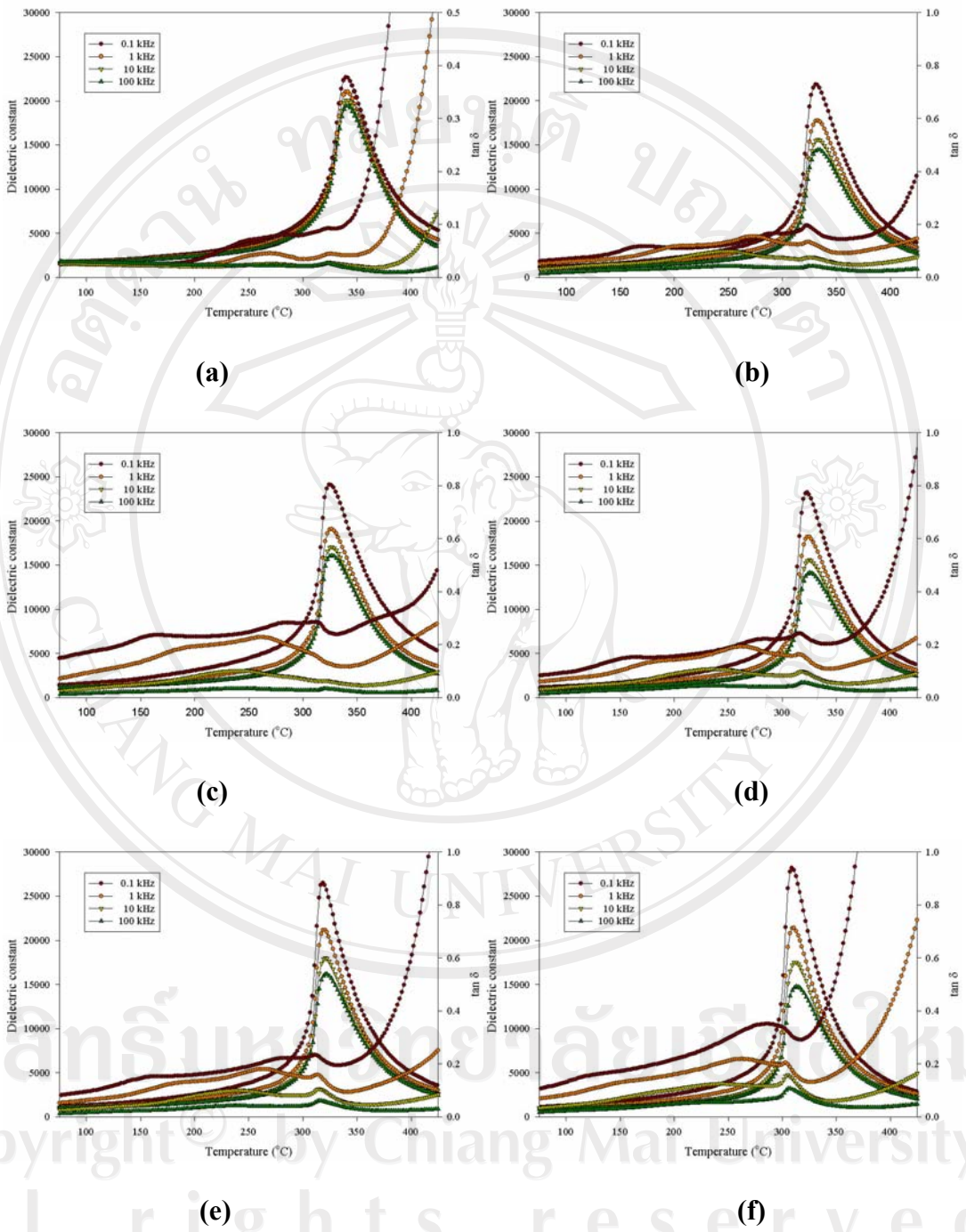


**Figure 5.3** Temperature and frequency dependence of dielectric properties of 0.2PZN–0.8PZT + $x$ wt% $MnO_2$ ceramics at 1200°C for 2h; (a) $x$ =0, (b) $x$ =0.1, (c) $x$ =0.3, (d) $x$ =0.5, (e) $x$ =0.7 and (f) $x$ =0.9.

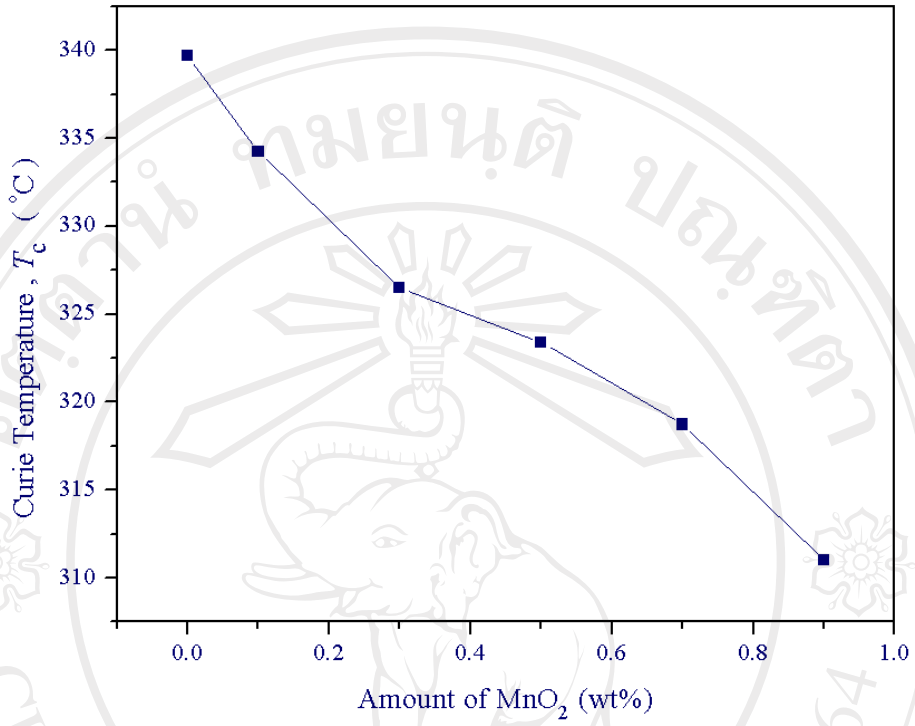


**Figure 5.4.** Curie temperature of the specimens sintered at 1200°C for 2h of 0.2PZN–0.8PZT + *x* wt% $MnO_2$ ceramics when *x* = 0 , 0.1 ,0.3 0.5, 0.7 and 0.9.

#### 5.1.2.3. Piezoelectric properties

Density, dielectric constant ($\varepsilon_r$), electromechanical coupling factor ($k_p$), mechanical quality factor ($Q_m$) and piezoelectric constant ($d_{33}$) are plotted as a function of amount of $MnO_2$ addition in Fig 5.5. When the amount of $MnO_2$ is lower than 0.5 wt%, density slightly increased. The $\varepsilon_r$, $k_p$ and $d_{33}$ show a decrease with increasing $MnO_2$ content. When the amount of $MnO_2$ is lower than 0.5 wt%, $k_p$ and $d_{33}$ are rapidly decreased with increasing $MnO_2$ content. It is well known that the substitutions of acceptor dopant Mn ions will lead to the creation of oxygen vacancies, which pin the movement of the ferroelectric domain walls and result in a decrease of $\varepsilon_r$, $k_p$ and $d_{33}$ [37, 106]. The mechanical quality factor ($Q_m$) are rapidly

increased with increasing $MnO_2$ content [100]. Therefore, the acceptor dopants of $MnO_2$ improve $Q_m$, significantly. The highest value $Q_m$ ( ~ 1413) are obtained in the ceramics with $MnO_2$ amounts of 0.5 wt%. Further addition of $MnO_2$ above 0.5 wt% leads to a slight decrease in the value of $Q_m$, which may be mainly attributable to non-uniformity of the microstructure, as shown in Fig.5.2.

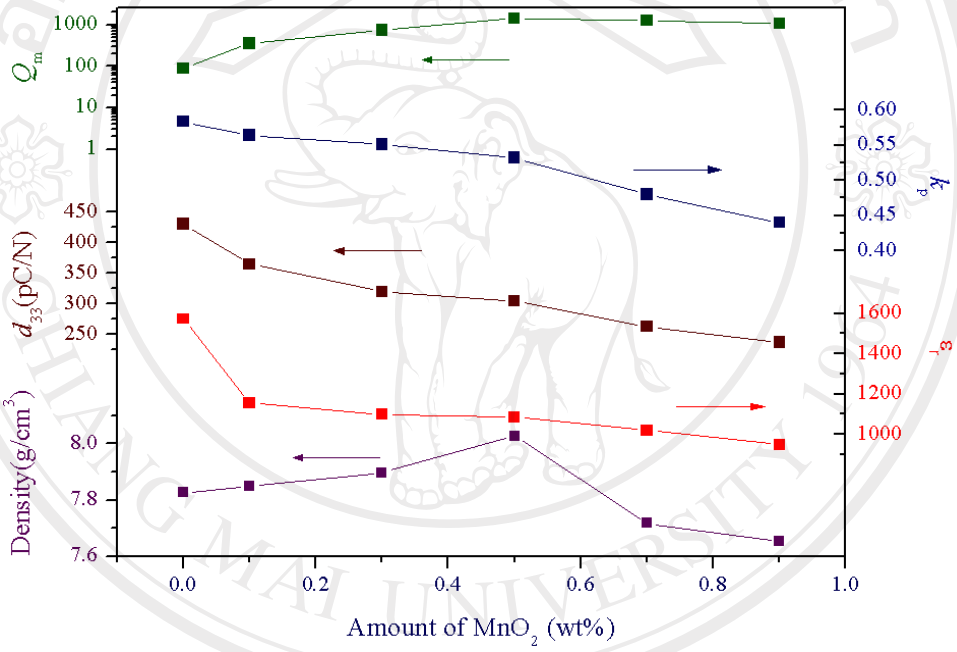


**Figure 5.5** Density, dielectric constant ($\varepsilon_r$), piezoelectric constant ($d_{33}$), electromechanical coupling factor ($k_p$), and mechanical quality factor ($Q_m$) of the specimens sintered at 1200°C for 2h of 0.2PZN–0.8PZT + $x$ wt% $MnO_2$ ceramics when $x$ = 0 , 0.1 ,0.3, 0.5, 0.7 and 0.9.

**Table 5.2** Dielectric and piezoelectric properties of 0.2PZN–0.8PZT + *x* wt% $MnO_2$ ceramics

| *x* | $T_C$ (°C) | Dielectric properties (at 25 °C, 1 kHz) | | Dielectric properties (at $T_m$) | | Piezoelectric properties | | |
|---|---|---|---|---|---|---|---|---|
| | | $\varepsilon_r$ | Tan$\delta$ | $\varepsilon_r$ | tan$\delta$ | $d_{33}$(pC/N) | $k_p$ | $Q_m$ |
| 0 | 339.7 | 1575 | 0.0249 | 21047 | 0.0420 | 430 | 0.583 | 90 |
| 0.1 | 334.2 | 1155 | 0.0436 | 17784 | 0.1181 | 365 | 0.564 | 356 |
| 0.3 | 326.5 | 1100 | 0.0464 | 19102 | 0.1241 | 320 | 0.551 | 735 |
| 0.5 | 323.4 | 1086 | 0.0440 | 18220 | 0.1454 | 305 | 0.532 | 1413 |
| 0.7 | 318.7 | 1020 | 0.0368 | 21178 | 0.1354 | 263 | 0.48 | 1260 |
| 0.9 | 311 | 948 | 0.0438 | 21389 | 0.1762 | 237 | 0.44 | 1080 |

### 5.1.2.4. Ferroelectric properties

The polarization-field (*P*–*E*) hysteresis loops 0.2PZN–0.8PZT + *x* wt% $MnO_2$ ceramics are shown in Fig. 5.6. The well-developed and fairly symmetric hysteresis loops with the field are observed for all compositions. To further assess ferroelectric characteristics in $MnO_2$-modified PZN-PZT ceramics, the ferroelectric parameters, i.e. the remnant polarization ($P_r$) and the coercive field ($E_c$), have been extracted from the experimental data, as given in Table 5.3. It can be seen clearly that $P_r$, $P_s$ decrease with an addition of $MnO_2$ into the PZN–PZT composition and $E_c$ increases to maximum at *x*=0.3 wt%. The ferroelectric characteristics can also be assessed with the hysteresis loop squareness ($R_{sq}$), as described earlier. As listed in Table 5.3, the loop squareness parameter $R_{sq}$ increases from 1.483 in *x*=0 to reach the maximum value of 1.712 in *x*=0.3. Further addition of $MnO_2$ above 0.3 wt% leads to a decrease in the loop squareness parameter, which are mainly attributable to non-uniformity of

the microstructure, as shown in Fig.5.2. The longitudinal strain (*s*) of the specimens as a function of the electric field is plotted in Fig. 5.7. The strains are degraded markedly when $MnO_2$ content is increased, as listed in Table 5.3.

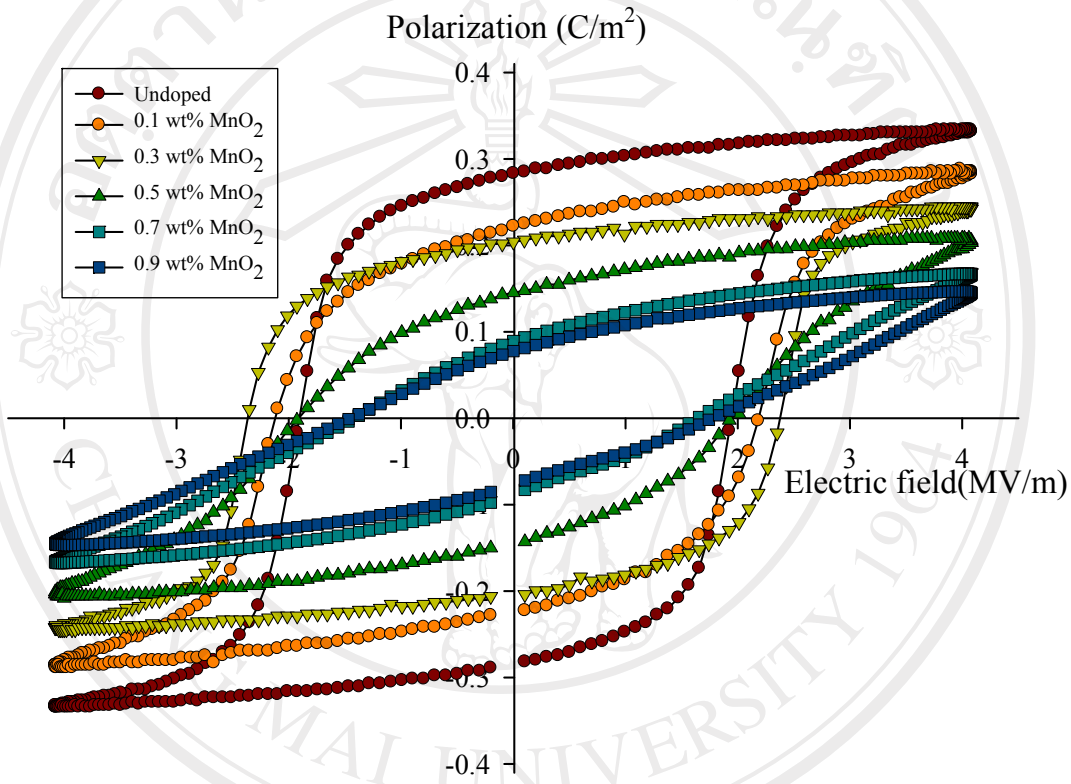


**Figure 5.6** Polarization and electric field of 0.2PZN–0.8PZT + *x* wt% $MnO_2$ ceramics.

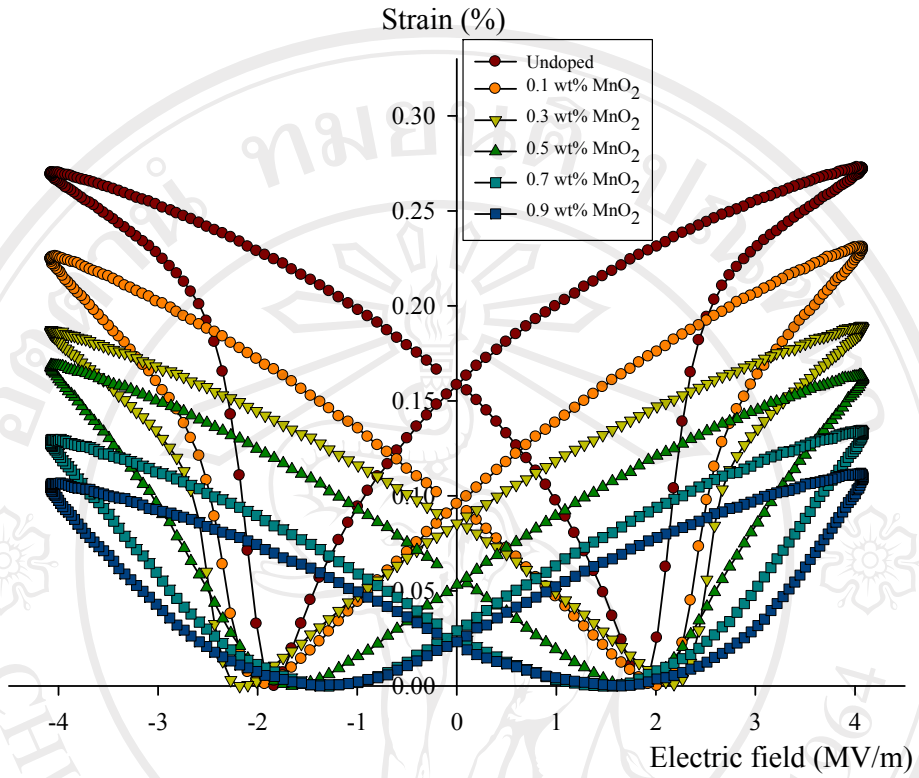


**Figure 5.7** Strain and electric field of 0.2PZN–0.8PZT + *x* wt% $MnO_2$ ceramics.

**Table 5.3** Ferroelectric and strain properties of 0.2PZN–0.8PZT + *x* wt% $MnO_2$ ceramics

| *x* | Ferroelectric properties (at 25 °C) | | | Loop squareness ($R_{sq}$) | Strain %@ 4MV/m |
|---|---|---|---|---|---|
| | $P_r$ (C/m$^2$) | $P_s$ (C/m$^2$) | $E_C$ (MV/m) | | |
| 0 | 0.287 | 0.300 | 1.97 | 1.483 | 0.278 |
| 0.1 | 0.224 | 0.233 | 2.18 | 1.488 | 0.231 |
| 0.3 | 0.208 | 0.213 | 2.37 | 1.712 | 0.188 |
| 0.5 | 0.147 | 0.175 | 1.94 | 1.024 | 0.162 |
| 0.7 | 0.089 | 0.126 | 1.63 | 0.811 | 0.134 |
| 0.9 | 0.077 | 0.111 | 1.75 | 0.811 | 0.115 |

These results clearly show decreased $P_r$ and strain level but increased $E_c$ with addition amount of $MnO_2$. This section shows the significance of $MnO_2$ addition in the electrical properties of the PZN–PZT system with ‘‘hard’’ characteristics presented. This observation could be caused from Mn ions which lead to the creation of oxygen vacancies, which in turn pin the movement of the ferroelectric domain walls, resulting in “hard” properties.

### 5.1.3. Summary

In this section, the dielectric, piezoelectric and ferroelectric properties of $MnO_2$-doped $0.2Pb(Zn_{1/3}Nb_{2/3})O_3$-$0.8Pb(Zr_{1/2}Ti_{1/2})O_3$ ceramics, which is the morphotropic phase boundary composition of the PZN-PZT system, were investigated. Crystal structure changed to rhombohedral side when increasing $MnO_2$ content. With the addition of $MnO_2$, Curie temperature $T_c$, the piezoelectric constant $d_{33}$ and electromechanical coupling factor $k_p$ were slightly decreased, but the mechanical quality factor $Q_m$ was significantly increased. The *P–E* and *s-E* loops demonstrated decreased $P_r$ and strain level but increased $E_c$ with increasing amount of $MnO_2$. These results clearly show the significance of $MnO_2$ addition in the controlling electrical properties of the PZN–PZT system to exhibit of ‘‘hard’’ characteristics.

## 5.2. Effect of $Fe_2O_3$ addition on properties PZN-PZT ceramics

Vittayakorn *et al.* [70] investigated processing conditions for producing phase-pure perovskite PZN–PZT ceramics with the conventional mixed-oxide method and B-site precursor. It was consistently shown that an MPB exists around $x = 0.25$ in this

binary system. It was clarified that the ceramics possess large electromechanical coupling factor $k_p$. But the mechanical quality factor $Q_m$ is too low to permit their use as high power piezoelectric devices. It is necessary to add some dopants on PZN–PZT based ceramics to optimize the piezoelectric properties for device applications [9, 45, 74, 85]. The influence of various substitutions on the B-site of $Pb(Zr,Ti)O_3$ perovskite has been widely investigated to optimize the piezoelectric properties [37, 99-101, 109]. Previously, in PZT with $Fe^{3+}$ doping, the dielectric loss (or tan δ) is usually reduced. This is especially true for the dielectric loss in a strong external field [102, 103, 110]. Therefore, $Fe^{3+}$ ion is an effective hard doping ion for PZT used in high-power transducers.

In this section, in order to develop PZN-PZT based ceramics for a piezoelectric transformer application, we investigate the effect of $Fe_2O_3$ addition on structure, and electrical properties of $0.2Pb(Zn_{1/3}Nb_{2/3})O_3$-$0.8Pb(Zr_{1/2}Ti_{1/2})O_3$ ceramics. The purpose of this section is to obtain ceramics with higher $d_{33}$, $k_p$ and $Q_m$, which are especially important from the viewpoint of the development of practical piezoelectric materials.



### 5.2.1. Experimental procedure

The specimens studied were fabricated according to the formula: $0.2Pb(Zn_{1/3}Nb_{2/3})O_3$-$0.8Pb(Zr_{1/2}Ti_{1/2})O_3$ + $x$ wt% $Fe_2O_3$, where x= 0.1, 0.3, 0.5, 0.7 and 0.9. Raw materials of PbO, $ZrO_2$, $TiO_2$, ZnO, $Nb_2O_5$ and $Fe_2O_3$ with >99% purity were used to prepare samples by a conventional mixed oxide process. The starting powders were mixied by zirconia ball media with isopropanal as a medium in a

polyethylene jar for 30 min via vibro-milling technique. The mixed slurry was dried and calcined at 900°C for 2h. The calcined powders were ball-milled again with additives and consolidated into disks of 12.5 mm diameter using isostatic pressing about 150 MPa. PbO-rich atmosphere sintering of the ceramics was performed in a high-purity alumina crucible at 1200 °C for 2h. As described in previous section, the sintered ceramics were characterized with the same procedures to determine the physical and electrical properties.

## 5.2.2. Results and discussion

### 5.2.2.1. Crystal structure, phase formations and microstructure

The XRD patterns of $0.2Pb(Zn_{1/3}Nb_{2/3})O_3$-$0.8Pb(Zr_{1/2}Ti_{1/2})O_3$ specimens with the addition of 0–0.9 wt% $Fe_2O_3$ are shown in Fig. 5.8. In these patterns, the crystal structure of the specimens is modified by the addition of $Fe_2O_3$, as revealed by the evaluation of (200) and (002) peaks. The perovskite structure appears to change to tetragonal side with increasing amount of $Fe_2O_3$. $Fe^{3+}$ ions are expected to substitute B-sites of the perovskite structure, because ionic radius of $Fe^{3+}$ is more similar to that of $Zr^{4+}$ , $Ti^{4+}$ , $Zn^{2+}$ and $Nb^{5+}$than that of $Pb^{2+}$ [23].

Figure 5.9 shows SEM photographs of the surfaces of $0.2Pb(Zn_{1/3}Nb_{2/3})O_3$-$0.8Pb(Zr_{1/2}Ti_{1/2})O_3$ ceramics doped with 0–0.9 wt% $Fe_2O_3$. As shown in Figs. 5.9 (a-e), the grain sizes of ceramics are increased with increasing amount of $Fe_2O_3$. However, the SEM micrographs in Fig.5.9 (f) show that a higher porosity level is observed when the amount of $Fe_2O_3$ is increased, which means that the specimens are not sintered effectively. The above results are obviously consistent with the change in

the bulk density with $Fe_2O_3$ content for Fe-doped $0.2Pb(Zn_{1/3}Nb_{2/3})O_3$-$0.8Pb(Zr_{1/2}Ti_{1/2})O_3$ ceramics. It should be noted that iron ions are possibly accumulate at the grain boundaries and inhibit grain growth due to the low solubilities of Fe ions in the lattice [31]. These inferences are obviously consistent with the changes mentioned above in the microstructures. The micrographs also show that the grain size of the ceramics varies considerably, as listed in Table 5.4.

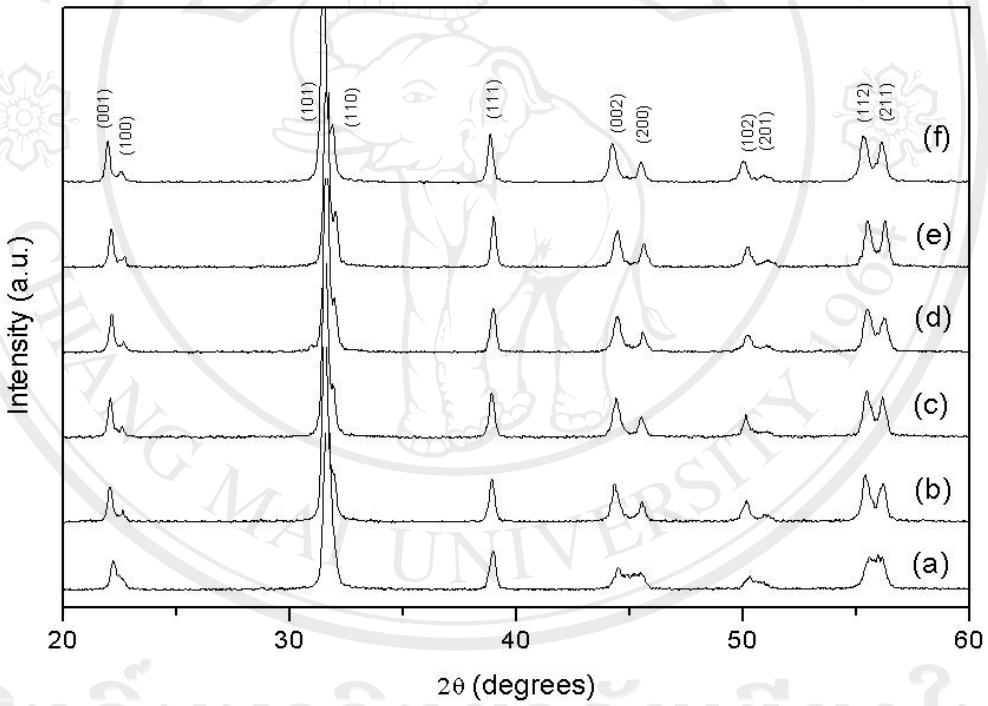


**Figure 5.8** XRD patterns of the samples sintered at 1200°C for 2h in 0.2PZN–0.8PZT + $x$ wt% $Fe_2O_3$ ceramics : (a) $x$ =0, (b) $x$ =0.1, (c) $x$ =0.3, (d) $x$ =0.5, (e) $x$ =0.7 and (f) $x$ =0.9.

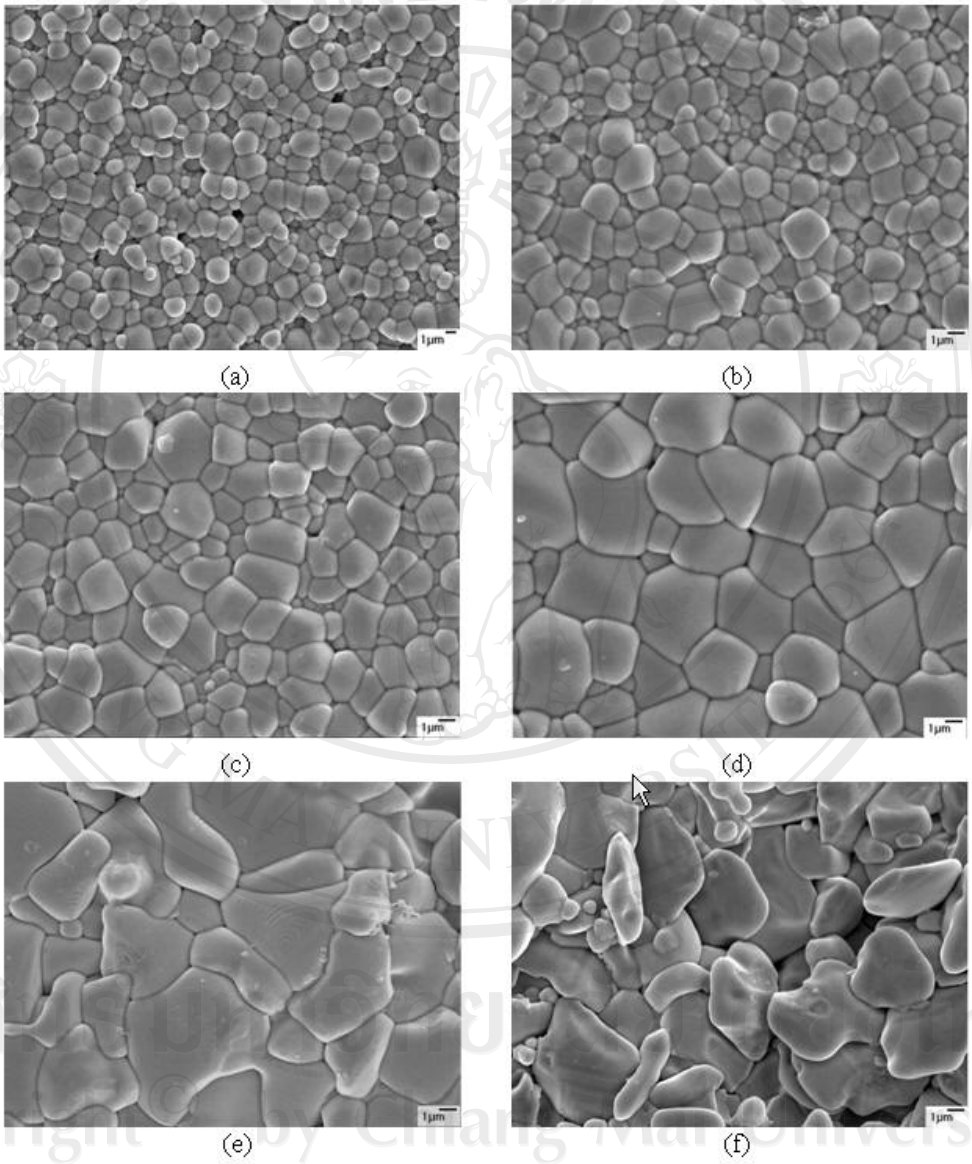


**Figure 5.9** SEM images of the specimens sintered surface of 0.2PZN–0.8PZT + $x$ wt% $Fe_2O_3$ ceramics at 1200°C for 2h;(a) $x$ =0, (b) $x$ =0.1, (c) $x$ =0.3, (d) $x$ =0.5, (e) $x$ =0.7 and (f) $x$ =0.9.

**Table 5.4** Physical properties of 0.2PZN–0.8PZT + *x* wt% $Fe_2O_3$ ceramics

| *x* | Density (g/cm$^3$) | Grain size range(μm) | Average grain size (μm) |
|---|---|---|---|
| 0 | 7.826 | 0.5 - 2.0 | 1.726 |
| 0.1 | 7.876 | 0.5 – 2.0 | 2.138 |
| 0.3 | 7.943 | 1.0 – 3.0 | 2.617 |
| 0.5 | 7.831 | 1.5 – 4.0 | 4.182 |
| 0.7 | 7.771 | 2.0 – 7.0 | 5.125 |
| 0.9 | 7.634 | 1.0 – 5.0 | 4.313 |

#### 5.2.2.2. Dielectric properties

The temperature and frequency dependence of the dielectric constant ($\varepsilon_r$) and dielectric loss tangent (tan δ) for 0.2PZN–0.8PZT + *x* wt% $Fe_2O_3$, *x* = 0, 0.1, 0.3, 0.5, 0.7 and 0.9 are shown in Fig. 5.10. The maximum dielectric constant at 1 kHz ($\varepsilon_m$ @ 1 kHz) is listed in Table 5.5. Dielectric behaviors show strong increase in frequency-dependence of dielectric constant and dielectric loss when increased amount of $Fe_2O_3$. This may be caused from oxygen vacancies and conducting regions near grain boundaries [108] with increasing $Fe_2O_3$ content. In Table 5.5, increasing amount of $Fe_2O_3$ is shown to decrease $\varepsilon_r$ at room temperature but increase $\varepsilon_m$ at Curie temperature. This observation may be related on grain size as effect observed previously in $BaTiO_3$ [111]. The variation of the Curie temperature ($T_c$) as a function of composition *x* is shown in Fig 5.11. The Curie temperature of 0.2PZN–0.8PZT + *x* wt% $Fe_2O_3$ system can be varied over a wide range from 310 to 340°C by controlling the addition of $Fe_2O_3$ content in the system.

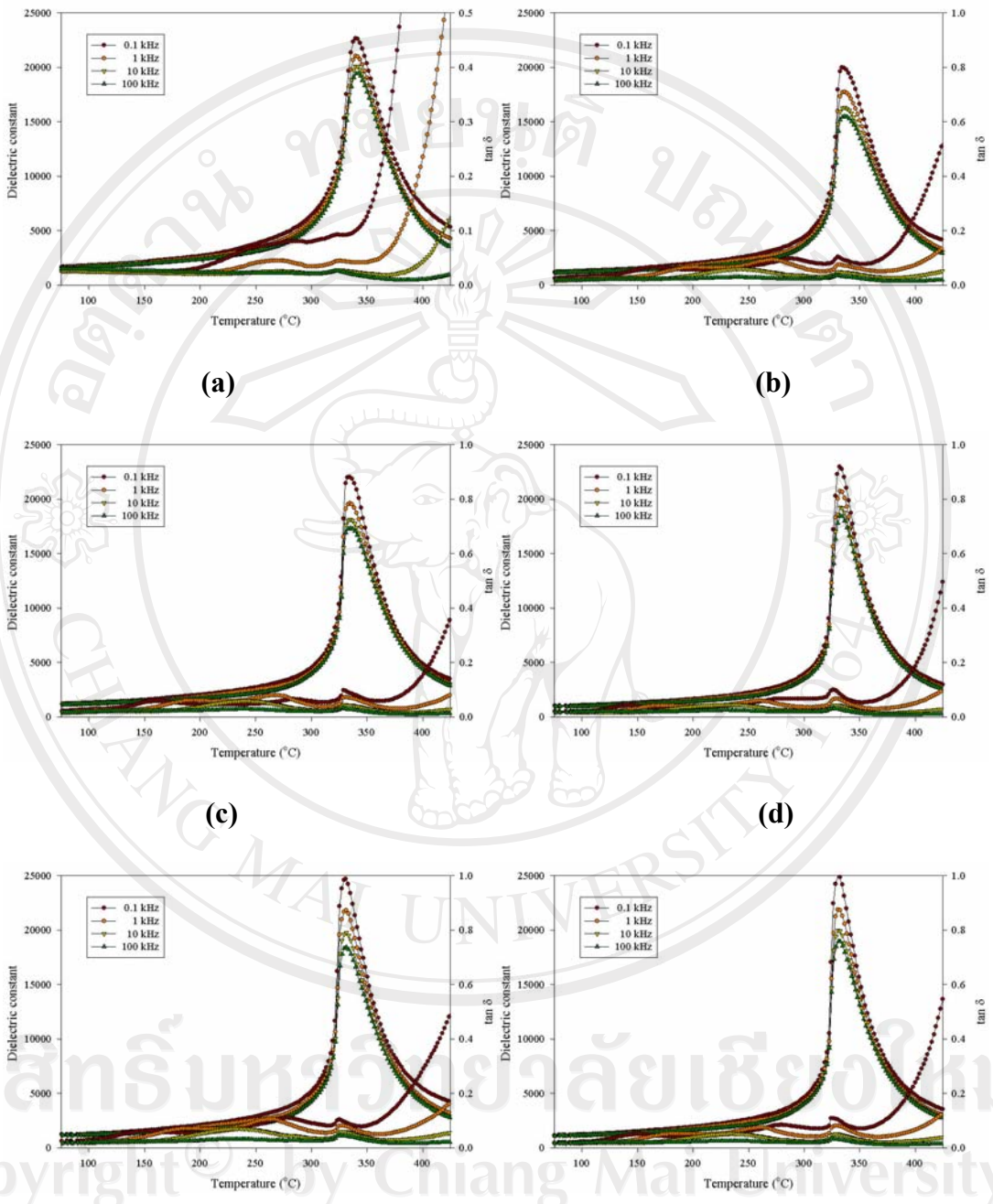


**Figure 5.10** Temperature and frequency dependence of dielectric properties of 0.2PZN–0.8PZT + $x$ wt% $Fe_2O_3$ ceramics at 1200°C for 2h; (a) $x$ =0, (b) $x$ =0.1, (c) $x$ =0.3, (d) $x$ =0.5, (e) $x$ =0.7 and (d) $x$ =0.9.

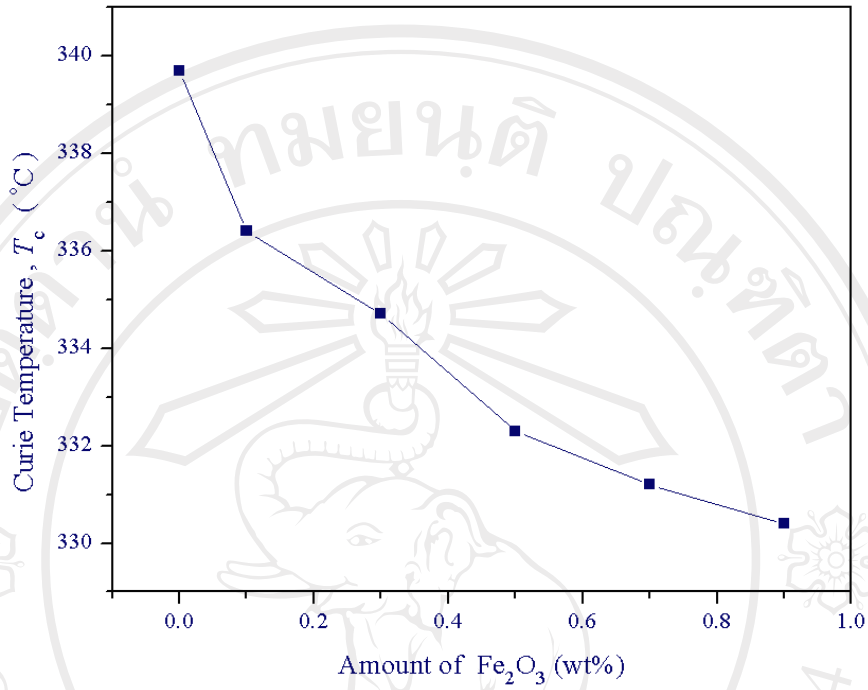


**Figure 5.11** Curie temperature of the specimens sintered at 1200°C for 2h of 0.2PZN–0.8PZT + $x$ wt% $Fe_2O_3$ ceramics when $x$ = 0 , 0.1 ,0.3 0.5, 0.7 and 0.9.

**Table 5.5** Dielectric and piezoelectric properties of 0.2PZN–0.8PZT + $x$ wt% $Fe_2O_3$ ceramics

| $x$ | $T_C$ (°C) | Dielectric properties (at 25 °C, 1 kHz) | | Dielectric properties (at $T_m$) | | Piezoelectric properties | | |
|---|---|---|---|---|---|---|---|---|
| | | $\varepsilon_r$ | tan$\delta$ | $\varepsilon_r$ | tan$\delta$ | $d_{33}$(pC/N) | $k_p$ | $Q_m$ |
| 0 | 339.7 | 1575 | 0.0249 | 21047 | 0.0420 | 430 | 0.58 | 90 |
| 0.1 | 336.4 | 1167 | 0.0175 | 17735 | 0.0716 | 355 | 0.55 | 98 |
| 0.3 | 334.7 | 1140 | 0.0159 | 19608 | 0.0698 | 331 | 0.51 | 110 |
| 0.5 | 332.3 | 1075 | 0.0180 | 20744 | 0.0608 | 310 | 0.47 | 128 |
| 0.7 | 331.2 | 921 | 0.0198 | 21819 | 0.0794 | 279 | 0.44 | 240 |
| 0.9 | 330.4 | 903 | 0.0179 | 21881 | 0.0814 | 213 | 0.41 | 356 |

#### 5.2.2.3. Piezoelectric properties

Figure 5.12 shows the changes in density, dielectric constant ($\varepsilon_r$), the piezoelectric constant ($d_{33}$) the electromechanical coupling factor ($k_p$) and the mechanical quality factor ($Q_m$) as a function of the amount of $Fe_2O_3$ addition, as also listed in Table 5.5. When the amount of $Fe_2O_3$ is lower than 0.3 wt%, density slightly increased. The $\varepsilon_r$ , $k_p$ and $d_{33}$ show a decrease with increasing $Fe_2O_3$ content. It is well known that the substitutions of acceptor dopant Fe ions will lead to the creation of oxygen vacancies, which in turn pin the movement of the ferroelectric domain walls [31, 74] and result in a decrease of $\varepsilon_r$ , $k_p$ and $d_{33}$. The mechanical quality factor ($Q_m$) are rapidly increased with increasing $Fe_2O_3$ content. The acceptor dopants of $Fe_2O_3$ improve $Q_m$, simultaneously. The highest value $Q_m$ ( ~ 356) are obtained in the ceramics with $Fe_2O_3$ amounts of 0.9 wt%. These results indicate that increased amount of $Fe_2O_3$ will degrade piezoelectric properties, due to exceeding the solution limit of Fe in the lattices [112,113].

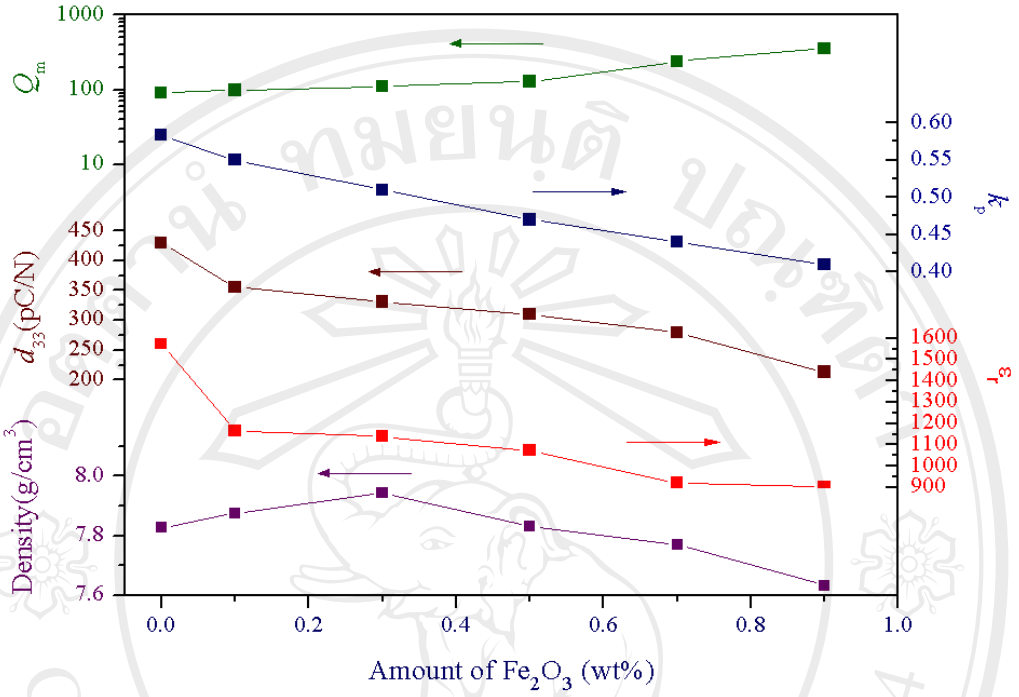


**Figure 5.12** Density, dielectric constant ($\varepsilon_r$), piezoelectric constant ($d_{33}$), electromechanical coupling factor ($k_p$), and mechanical quality factor ($Q_m$) of the specimens sintered at 1200°C for 2h in 0.2PZN–0.8PZT + $x$ wt% $Fe_2O_3$ ceramics; when $x$ = 0 , 0.1 ,0.3, 0.5, 0.7 and 0.9.

#### 5.2.2.4. Ferroelectric properties

The polarization-field ($P$–$E$) hysteresis loops of 0.2PZN–0.8PZT + $x$ wt% $Fe_2O_3$ ceramics are shown in Fig. 5.13. The well-developed and fairly symmetric hysteresis loops with the field are observed for all compositions. To further assess ferroelectric characteristics in $Fe_2O_3$–modified PZN-PZT ceramics, the ferroelectric parameters, i.e. the remnant polarization ($P_r$) and the coercive field ($E_c$), have been extracted from the experimental data, as listed given in Table 5.6. It can be seen clearly that $P_r$ and $P_s$ decrease, while $E_c$ increases, with an addition of $Fe_2O_3$ into the

PZN–PZT composition. The ferroelectric characteristics of the ceramics can also be assessed with the hysteresis loop squareness ($R_{sq}$), as described in earlier sections. As listed in Table 5.6, the loop squareness parameter $R_{sq}$ increases from 1.483 in $x$=0 to reach the maximum value of 1.761 in $x$=0.5. Further addition of $Fe_2O_3$ above 0.5 wt% leads to a decrease in the loop squareness parameter, which is mainly attributable to abnormal grain of the microstructure, as shown in Fig. 5.9. Strain of specimens as a function of the electric field was shown in Figs. 5.14, which show decreasing strain and increasing coercive field with $Fe_2O_3$ content, as also listed in Table 5.6.

**Table 5.6** Ferroelectric and strain properties of 0.2PZN–0.8PZT + $x$ wt% $Fe_2O_3$ ceramics

| $x$ | Ferroelectric properties (at 25 °C) | | | Loop squareness ($R_{sq}$) | Strain % @ 4MV/m |
|---|---|---|---|---|---|
| | $P_r$ (C/m$^2$) | $P_s$ (C/m$^2$) | $E_C$ (MV/m) | | |
| 0 | 0.287 | 0.300 | 1.97 | 1.483 | 0.278 |
| 0.1 | 0.257 | 0.267 | 2.14 | 1.702 | 0.268 |
| 0.3 | 0.253 | 0.262 | 2.25 | 1.732 | 0.254 |
| 0.5 | 0.251 | 0.254 | 2.28 | 1.761 | 0.234 |
| 0.7 | 0.239 | 0.249 | 2.35 | 1.650 | 0.223 |
| 0.9 | 0.227 | 0.243 | 2.38 | 1.661 | 0.207 |

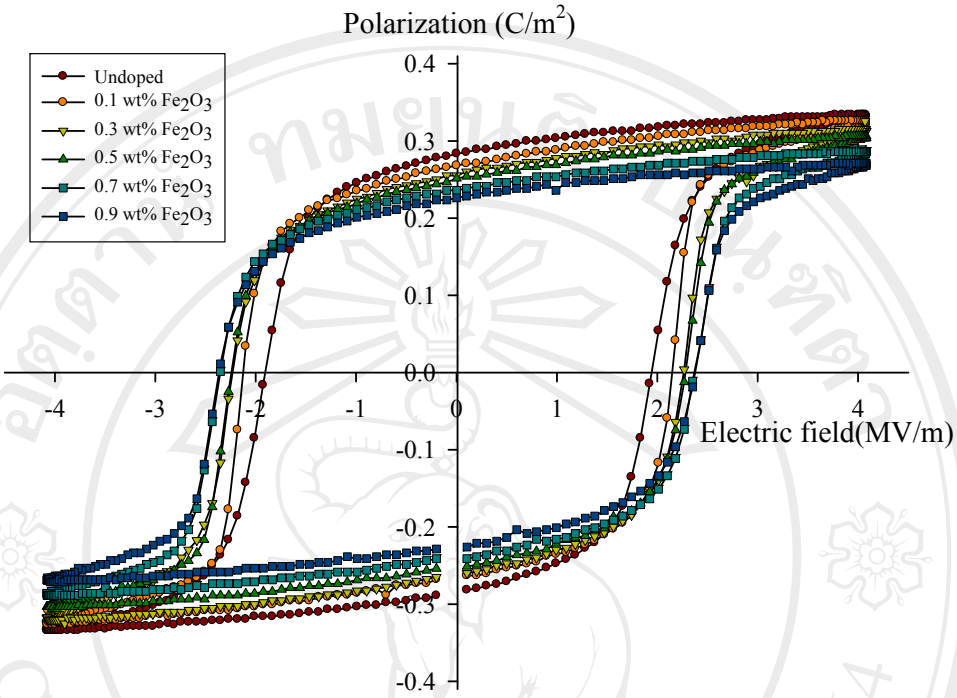


**Figure 5.13** Polarization and electric field 0.2PZN–0.8PZT + *x* wt% $Fe_2O_3$ ceramics.

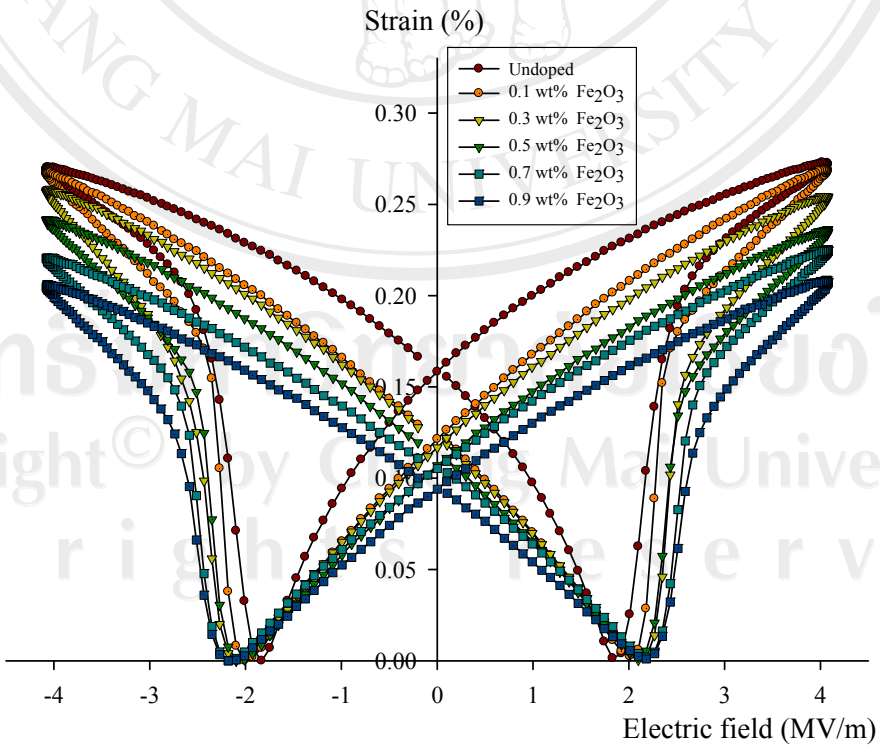


**Figure 5.14** Strain and electric field of 0.2PZN–0.8PZT + *x* wt% $Fe_2O_3$ ceramics.

These results that show decreased $P_r$ and strain level but increased $E_c$ when addition amount of $Fe_2O_3$, clearly indicate the significance of $Fe_2O_3$ addition in the electrical properties of the PZN–PZT system with ‘‘hard’’ characteristics. This observation could be caused by Fe-ions addition that leads to the creation of oxygen vacancies, which then pin the movement of the ferroelectric domain walls.

### 5.2.3. Summary

In this section, the dielectric, piezoelectric and ferroelectric properties of $Fe_2O_3$-doped $0.2Pb(Zn_{1/3}Nb_{2/3})O_3$-$0.8Pb(Zr_{1/2}Ti_{1/2})O_3$ ceramics, which is the morphotropic phase boundary composition of the PZN-PZT system, were investigated. Crystal structure changes to tetragonal side with increasing $Fe_2O_3$ content. With the addition of $Fe_2O_3$, Curie temperature $T_c$, the piezoelectric constant $d_{33}$ and electromechanical coupling factor $k_p$ were slightly decreased, but the mechanical quality factor $Q_m$ was significantly increased. The *P–E* and *s-E* loops show that decreased $P_r$ and strain level but increased $E_c$ when addition amount of $Fe_2O_3$. These results clearly showed the significance of $Fe_2O_3$ addition in the electrical properties of the PZN–PZT system with ‘‘hard’’ characteristics.

## 5.3. Comparison between $Fe_2O_3$ and $MnO_2$ addition on properties of PZN-PZT ceramics

Very small amounts addition of $MnO_2$ [98, 99] and $Fe_2O_3$ [112, 113] are well known to be effective in for improving the reliability of ceramic capacitors. The enhanced properties are expected to be due to the distribution of $Mn^{2+}$, $Mn^{3+}$, and

$Mn^{4+}$ or $Fe^{3+}$ on B-sites. Mn, Fe incorporated on the B-sites would act as a lower valent species on a higher valent site. Accordingly, oxygen vacancies would be created for charge compensation, imparting polarization pinning and ‘‘hard’’ characteristics, i.e., an increase in $Q_m$ value [ 102-105, 113].

In this section, we investigate the effect of $Fe_2O_3$ and $MnO_2$ addition on structure, and electrical properties of $0.2Pb(Zn_{1/3}Nb_{2/3})O_3$-$0.8Pb(Zr_{1/2}Ti_{1/2})O_3$ ceramics. The purpose of this section is to directly compare electrical properties of updoped with $Fe_2O_3$- and $MnO_2$-doped PZN-PZT ceramics, which are especially important from the viewpoint of the development of practical piezoelectric materials.

### 5.3.1. Experimental procedure

The specimens studied were fabricated according to the formula: $0.2Pb(Zn_{1/3}Nb_{2/3})O_3$-$0.8Pb(Zr_{1/2}Ti_{1/2})O_3$ + 0.5 mol% metal oxide, which are $MnO_2$ and $Fe_2O_3$. Raw materials of PbO, $ZrO_2$, $TiO_2$, ZnO, $Nb_2O_5$, $MnO_2$ and $Fe_2O_3$ with >99% purity were used to prepare samples by a conventional mixed oxide process. The starting powders were mixied by zirconia ball media with isopropanal as a medium in a polyethylene jar for 30 min via vibro-milling technique. The mixed slurry was dried and calcined at 900$^o$C for 2h. The calcined powders were ball-milled again with additives and consolidated into disks of 12.5 mm diameter using isostatic pressing about 150 MPa. PbO-rich atmosphere sintering of the ceramics was performed in a high-purity alumina crucible at 1200 °C for 2h. The prepared specimens were then characterized, physically and electrically, with the same procedures described in previous sections.

## 5.3.2. Results and discussion

### 5.3.2.1. Crystal structure, phase formations and microstructure

The XRD patterns of updoped, and $Fe_2O_3$- and $MnO_2$-doped $0.2Pb(Zn_{1/3}Nb_{2/3})O_3$-$0.8Pb(Zr_{1/2}Ti_{1/2})O_3$ specimens are shown in Fig.5.15. The pyrochlore phase is not observed in this system at all. In undoped composition, XRD pattern show the co-existence of the rhombohedral and tetragonal phase, indicating MPB composition. When adding 0.5 mol% of $Fe_2O_3$ and $MnO_2$, crystal structures were shifted away from MPB to tetragonal and rhombohedral, respectivity [98, 112].

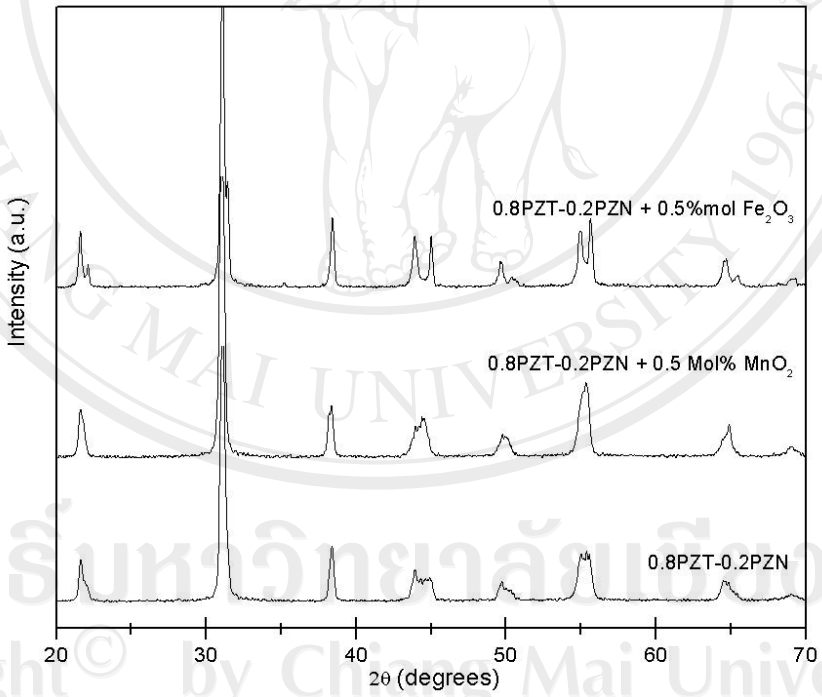


**Figure 5.15** XRD patterns of the samples sintered at 1200°C for 2h in 0.2PZN–0.8PZT ceramics: (a)undoped, (b) doped with 0.5mol% $MnO_2$ and (c) doped with 0.5mol% $Fe_2O_3$.

Figure 5.16 shows SEM photographs of the surfaces of undoped and doped $0.2Pb(Zn_{1/3}Nb_{2/3})O_3$-$0.8Pb(Zr_{1/2}Ti_{1/2})O_3$ ceramics. As shown in Fig. 5.16, the average grain sizes of ceramics are increased with addition of $MnO_2$ and $Fe_2O_3$. It is believed that Mn and Fe ions are mainly incorporated into the lattice [104 ,113], which results in more grain-growth mechanism. The micrographs also show that the grain size of the ceramics varies considerably from 1 to 3 μm, as listed in Table 5.7. These inferences are obviously consistent with the changes mentioned above in the microstructures.

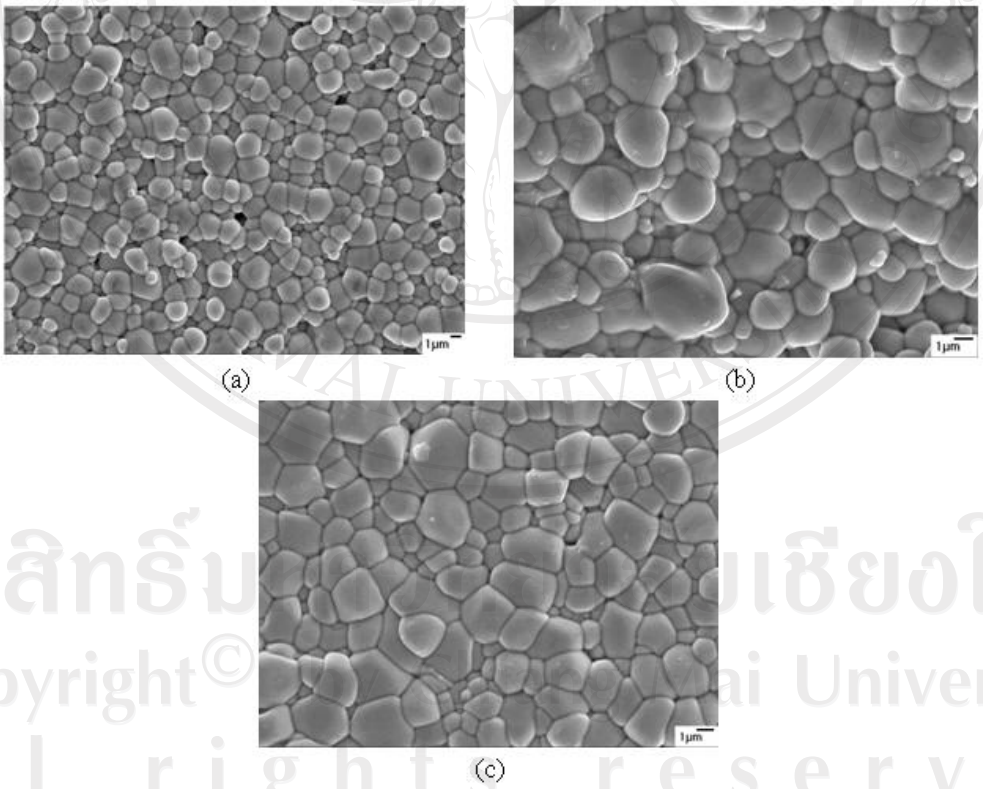




**Figure 5.16** SEM images of the specimens sintered surface of 0.2PZN–0.8PZT ceramics at 1200°C for 2h; (a) undoped, (b) doped with 0.5 mol% $MnO_2$ and (c) doped with 0.5 mol% $Fe_2O_3$**.**

**Table 5.7** Physical properties of 0.2PZN–0.8PZT ceramics

| *Composition* | Density (g/cm$^3$) | Grain size range(μm) | Average grain size (μm) |
|---|---|---|---|
| Undoped | 7.826 | 0.5 - 2.0 | 1.726 |
| 0.5 mol% $MnO_2$ | 7.897 | 1.0 – 3.0 | 2.991 |
| 0.5 mol% $Fe_2O_3$ | 7.943 | 1.0 – 3.0 | 2.617 |

### 5.3.2.2. Dielectric properties

Figure 5.17 shows the dielectric constant ($\varepsilon_r$) and dielectric loss tangent ($\tan\delta$) as a function of temperature and frequency for all the compositions. Fig. 5.17 (b-c) shows strong frequency dependence of the maximum dielectric constant in $MnO_2$-doped and $Fe_2O_3$- doped. This observation is attributed to the creation of oxygen vacancies and conducting regions near grain boundaries [108]. In Table 5.8, doping of $Fe_2O_3$ and $MnO_2$ decreases $\varepsilon_r$ at room temperature, but increases $\varepsilon_m$ at Curie temperature. This may be explained by grain size effect, as reported earlier for $BaTiO_3$ [111]. The Curie temperature ($T_C$) of the specimens decreases with $MnO_2$ and $Fe_2O_3$ doping. For undoped speciemen, $T_C$ = 339.7 °C is observed while for $MnO_2$-doped and $Fe_2O_3$-doped, the $T_C$ are 332.9 °C and 335.9 °C, indicating that these two compositions move away from MPB region.

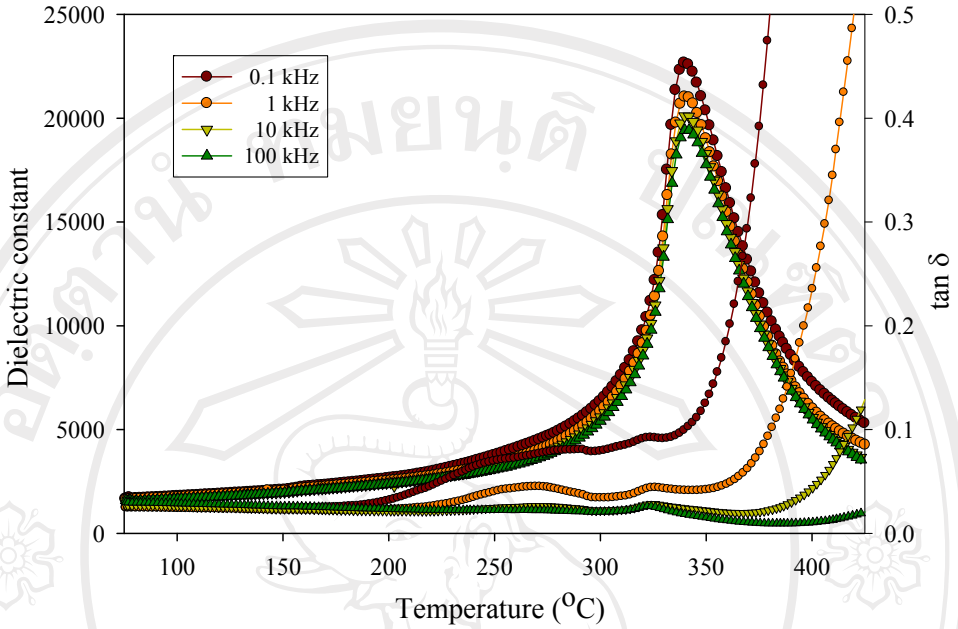


**(a)**

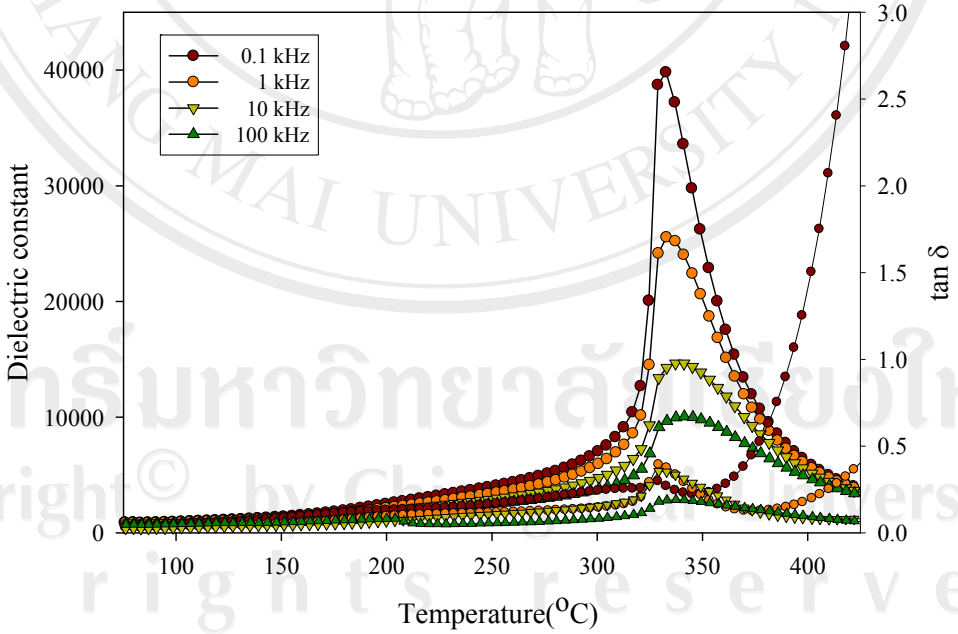


**(b)**

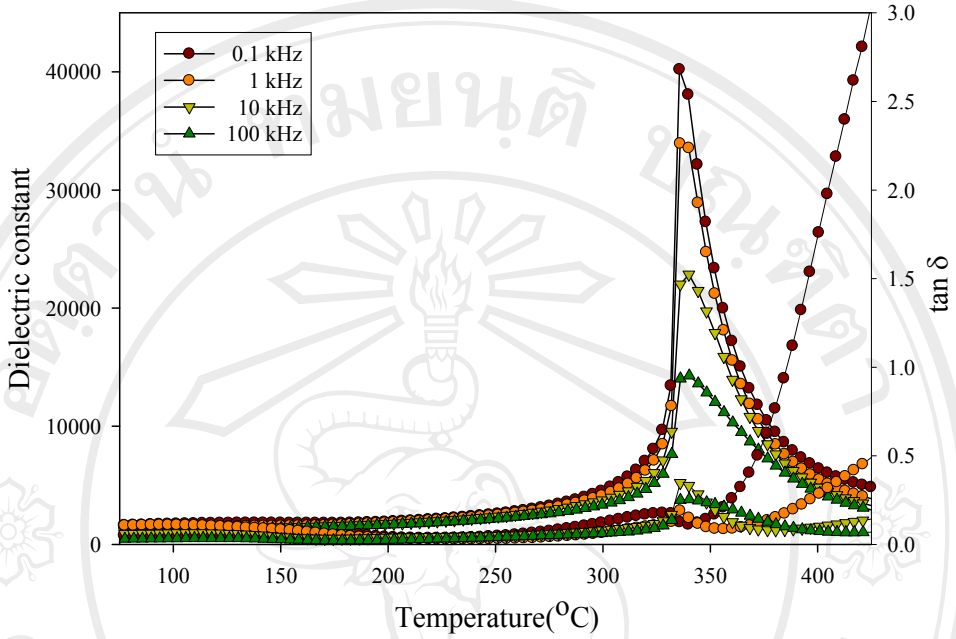


**(c)**

**Figure 5.17** Temperature and frequency dependence of dielectric properties of 0.2PZN–0.8PZT ceramics at 1200°C for 2h : (a) undoped, (b) doped with 0.5 mol% $MnO_2$ and (c) doped with 0.5 mol% $Fe_2O_3$ .

**Table 5.8** Dielectric and piezoelectric properties of 0.2PZN–0.8PZT ceramics

| ***Composition*** | $T_C$ (°C) | **Dielectric properties (at 25 °C, 1 kHz)** | | **Dielectric properties (at $T_{Max}$)** | | **Piezoelectric properties** | | |
|---|---|---|---|---|---|---|---|---|
| | | $\varepsilon_r$ | tan$\delta$ | $\varepsilon_r$ | tan$\delta$ | $d_{33}$(pC/N) | $k_p$ | $Q_m$ |
| Undoped | 339.7 | 1575 | 0.0249 | 21047 | 0.0420 | 430 | 0.583 | 90 |
| 0.5 mol%$MnO_2$ | 332.9 | 837 | 0.0310 | 25551 | 0.3765 | 320 | 0.551 | 735 |
| 0.5 mol% $Fe_2O_3$ | 335.9 | 1272 | 0.0997 | 33941 | 0.1907 | 331 | 0.513 | 110 |

#### 5.3.2.3. Piezoelectric properties

Table 5.8, shows the changes in density, dielectric constant ($\varepsilon_r$), the piezoelectric constant ($d_{33}$) the electromechanical coupling factor ($k_p$) and the mechanical quality factor ($Q_m$). With addition of $Fe_2O_3$ and $MnO_2$, density slightly increased. The $\varepsilon_r$, $k_p$ and $d_{33}$ show a decrease with addition of $Fe_2O_3$ and $MnO_2$. It is well known that the substitutions of acceptor dopant Mn and Fe ions will lead to the creation of oxygen vacancies [31,74], which pin the movement of the ferroelectric domain walls and result in a decrease of $\varepsilon_r$, $k_p$ and $d_{33}$. The mechanical quality factor ($Q_m$) are slightly increased with additional of dopants [98, 105].

#### 5.3.2.4. Ferroelectric properties

The polarization-field ($P$–$E$) hysteresis loops of 0.2PZN–0.8PZT ceramics are shown in Fig. 5.18. The well-developed and fairly symmetric hysteresis loops with the field are observed for all compositions. To further assess ferroelectric characteristics in $Fe_2O_3$ and $MnO_2$ modified PZT ceramics, the ferroelectric parameters, i.e. the remnant polarization ($P_r$) and the coercive field ($E_c$), have been extracted from the experimental data given in Table 5.9. It can be seen clearly that $P_r$ decreases but $E_c$ increases with an addition of $Fe_2O_3$ and $MnO_2$ into the 0.2PZN–0.8PZT composition. The ferroelectric characteristics of the ceramics can also be assessed with the hysteresis loop squareness ($R_{sq}$), as mentioned previously. As listed in Table 5.9, the loop squareness parameter $R_{sq}$ increases with addition of $Fe_2O_3$ and $MnO_2$.

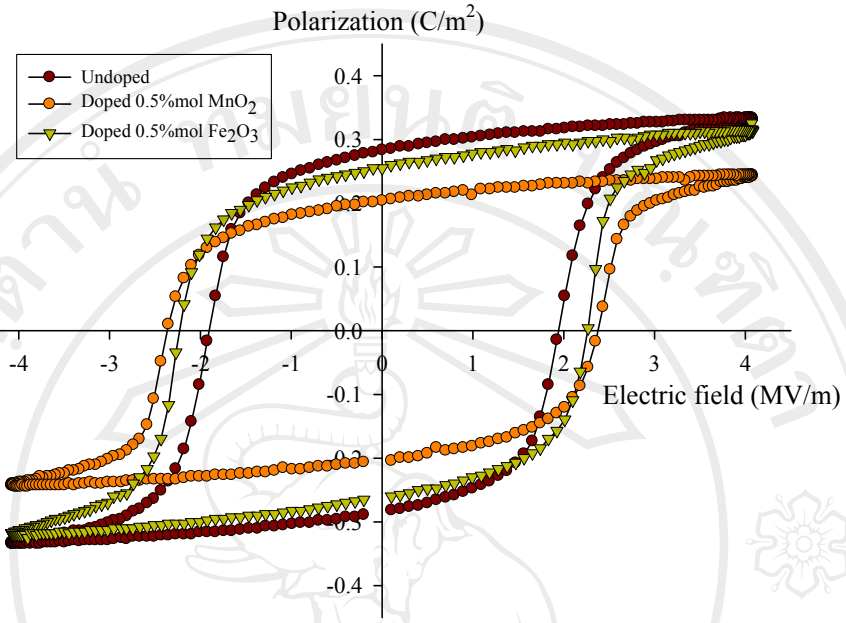


**Figure 5.18** Polarization as a function of electric field of 0.2PZN–0.8PZT ceramics in condition of undoped, doped with 0.5 mol% $MnO_2$ and doped with 0.5 mol% $Fe_2O_3$.

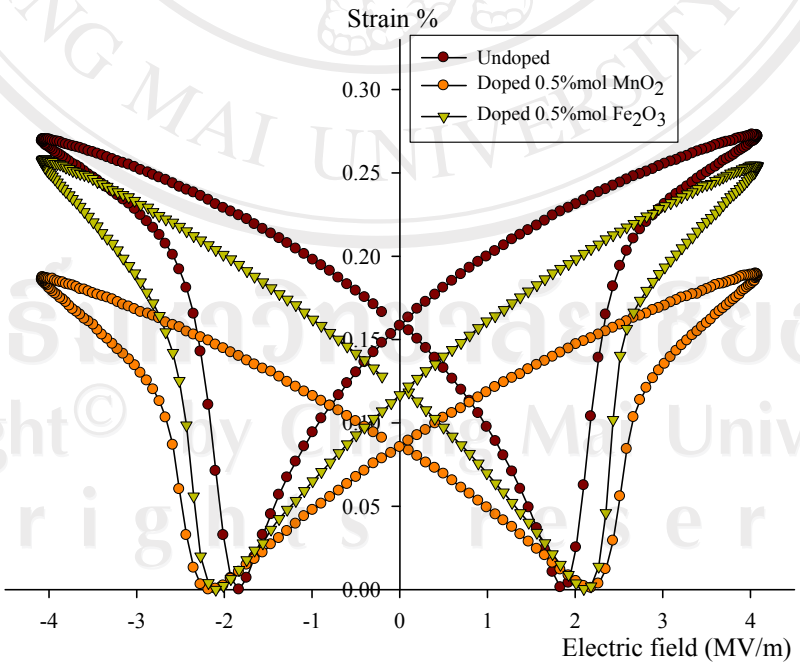


**Figure 5.19** Strain as a function of electric field of 0.2PZN–0.8PZT ceramics in condition of undoped, doped with 0.5 mol% $MnO_2$ and doped with 0.5 mol% $Fe_2O_3$.

Strain of specimens as function of the electric filed, displayed in Fig. 5.19, show decreasing strain and increasing coercive field addition of $Fe_2O_3$ and $MnO_2$ as also listed in Table 5.9.

**Table 5.9** Ferroelectric and strain properties of 0.2PZN–0.8PZT ceramics

| *Composition* | Ferroelectric properties (at 25 °C) | | | Loop squareness ($R_{sq}$) | Strain % @ 4MV/m |
|---|---|---|---|---|---|
| | $P_r$ (C/m$^2$) | $P_s$ (C/m$^2$) | $E_C$ (MV/m) | | |
| Undoped | 0.287 | 0.300 | 1.97 | 1.483 | 0.278 |
| 0.5 mol% $MnO_2$ | 0.208 | 0.213 | 2.37 | 1.712 | 0.188 |
| 0.5 mol% $Fe_2O_3$ | 0.253 | 0.262 | 2.25 | 1.732 | 0.254 |

These results show that influence of Mn-ion is more effective in harden properties of PZN-PZT than Fe-ion because $MnO_2$ may create $Mn^{2+}$, and $Mn^{3+}$ at high temperature [114], that leads to the creation of oxygen vacancies in higher concentration, as compared to Fe-ion.

### 5.3.3. Summary

In this section, the dielectric piezoelectric and ferroelectric properties of $Fe_2O_3$ and $MnO_2$-doped $0.2Pb(Zn_{1/3}Nb_{2/3})O_3$-$0.8Pb(Zr_{1/2}Ti_{1/2})O_3$ were investigated. In case of addition of $Fe_2O_3$, the crystal structure was shifted to tetragonal phase. On the other hand, addition of $MnO_2$ shifted the crystal structure to rhombohedral. With addition of $Fe_2O_3$ or $MnO_2$, Curie temperature $T_c$, the piezoelectric constant $d_{33}$ and electromechanical coupling factor $k_p$ were slightly decreased, but the mechanical quality factor $Q_m$ was significantly increased. Polarization and strain characteristics were shown with increasing $E_c$, decreasing of $P_r$, $P_s$ and strain indicating hardening effect with $Fe_2O_3$ and $MnO_2$ addition.